Proceedings of the ASME 2014 Dynamic Systems and Control Conference
DSCC2014
October 22-24, 2014, San Antonio, TX, USA

DSCC2014-6175

LOCATION ISOLABILITY OF INTAKE AND EXHAUST MANIFOLD LEAKS IN A TURBOCHARGED DIESEL ENGINE WITH EXHAUST GAS RECIRCULATION

Michael J. Hand, III*
Electrical Engineering
University of Michigan
Ann Arbor, Michigan 48109
Email: mikehand@umich.edu

Anna Stefanopoulou
Mechanical Engineering
University of Michigan
Ann Arbor, Michigan 48109

ABSTRACT

An investigation into the isolability of the location of intake and exhaust manifold leaks in heavy duty diesel engines is presented. In particular, established fault detection and isolation (FDI) methods are explored to assess their utility in successfully determining the location of a leak within the air path of an engine equipped with exhaust gas recirculation and an asymmetric twin-scroll turbine. It is further shown how consideration of the system's variation across multiple operating points can lead to improved ability to isolate the location of leaks in the intake and exhaust manifolds.

NOMENCLATURE

VARIABLES AND QUANTITIES

A	Area (m^2)	CoV	Coeff. of variation (-)
J	Inertia (kgm^2)	N	Speed (rpm)
P	Pressure (Pa)	R	Gas const. (J/kgK)
r	Asymmetry ratio (-) or residual	T	Temperature (K)
V	Volume (m^3)	W	Mass flow (kg/s)
γ	Spec. heat ratio (-)	λ	Normalized air-fuel ratio (-)
μ	Mean value (same as quantity)	Π	Pressure ratio (-)
σ	Standard deviation (same as quantity)	Ψ	Flow parameter (-)

SUBSCRIPTS AND ABBREVIATIONS

a	Air	amb	Ambient
c	Compressor	d	Displacement
EGR	Exhaust gas recirc.	e	Engine
ei	Engine/cylinder in	em	Exhaust manifold
ems	Small scroll ex. man.	eml	Large scroll ex. man.
eo	Engine/cylinder out	ex	Exhaust
f	Fuel	im	Intake manifold
in	Into the volume	out	Out of the volume
s	Stoichiometric	ss	Steady state
t	Turbine	tc	Turbocharger
tl	Large turbine scroll	ts	Small turbine scroll
u	Control signal	w	Exogenous input
x	State variable/vector	vol	Volumetric
WG	Wastegate	$\bar{\cdot}$	Measured quantity
$\hat{\cdot}$	Estimated quantity		

1 INTRODUCTION

Over the past thirty years, regulations on automotive diesel engine systems have become increasingly strict. These regulations include emissions standards as well as requirements for successful detection of certain classes of faults. While initially only faults that posed a safety hazard needed to be diagnosed, more recent regulations also include on-board diagnosis (OBD) of faults that may increase emissions beyond a given threshold [1]. These faults include sensor failures, manifold leaks, and stuck or slow actuators, among others. Meanwhile, manufacturers have worked to increase the efficiency of the engine systems, often resulting in increased complexity, which simple models struggle to capture well. Since faults are typically viewed as deviations from the expected behavior, the expected behavior must be well understood for a diagnostic system to be effective.

A recent overview of various techniques for fault diagnostics in engines is presented in [2]. Model-based approaches, like

*Address all correspondence to this author.

those used in this work, make use of the available knowledge of the system behavior to allow successful detection and isolation of faults using analytical redundancy from the model equations, rather than relying on duplication of physical sensors [3].

Model-based fault detection and isolation (FDI) for nonlinear systems, such as the considered diesel engine, is a young field. Still, a number of advancements have been made recently, especially in response to increasing demand for reliable, inexpensive automotive fault detection systems. The work presented here builds on the techniques from model-based approaches, similar to those used in [3–5], among others.

Previous works, such as [5, 6], have investigated the detectability of manifold leaks, particularly intake manifold leaks, and whether they can be isolated from a number of other types of faults (e.g. sensor and actuator failures). These works have shown good detectability of leak faults, as well as a reasonable ability to isolate leaks from other classes of faults. To the best of the authors' knowledge no such analysis is presented in the literature for isolating intake manifold leaks from exhaust manifold leaks. While leaks in the actual manifold wall are unlikely to form, there are a number of joints and connections present in the engine system that are susceptible to such leaks. These include the connection of the EGR path to one of the manifolds or the connection between the charge cooler to the intake manifold. Some examples of potential leak locations are indicated by the red stars in the engine schematic in Fig. 1. It would be desirable for FDI systems to be able to determine the manifold in which a leak has occurred , as the material present in the exhaust manifold is more polluting than that in the intake manifold. Further, the emissions impact of an intake manifold leak may be partially accommodated by closing the EGR valve. By significantly reducing the flow of combustion products into the leaking manifold, the environmental impact of the fault would be reduced until the engine could be serviced.

The paper is organized as follows: Section 2 describes the considered engine and the model thereof; Section 3 explores the effects of intake and exhaust manifold leaks on the engine operation; Section 4 presents an analysis and comparison of isolation strategies for determining the source of a leak; conclusions and future work are presented in Section 5.

2 ENGINE SYSTEM

The considered approach to fault diagnosis—model-based diagnosis—uses an explicit mathematical model to calculate the expected behavior based on sensors and known actuators. Accordingly, a good model of the system behavior is indispensable for reliable fault diagnosis.

2.1 System Description

The considered engine is a Detroit Diesel 13-liter 6-cylinder heavy duty diesel engine, which is equipped with an asymmetric twin-scroll turbine, an electronically actuated exhaust gas recirculation (EGR) valve, and a pneumatically actuated wastegate (WG) valve, which bypasses the turbine. One of the unique features of this engine is the asymmetric twin-scroll turbine, which helps mitigate the tradeoffs between smoke generation, NO_x generation, and efficiency [7].

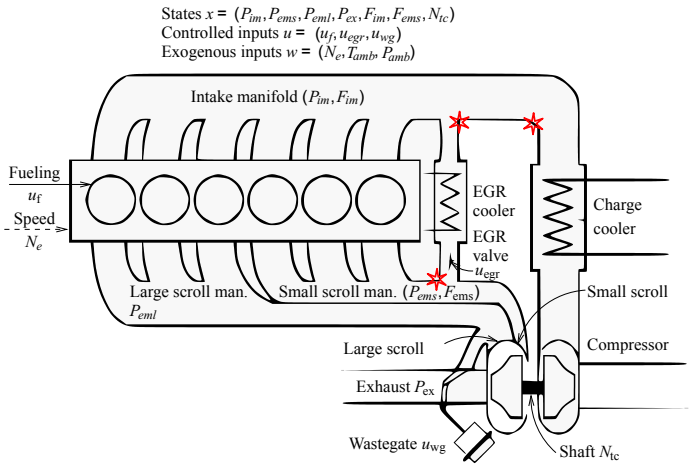

FIGURE 1. SCHEMATIC OF THE ENGINE AND OVERVIEW OF THE MODEL STATES, CONTROLLED INPUTS, AND EXOGENOUS INPUTS.

2.2 Model Description

This model was designed and calibrated in [7] and the equations are summarized in Appendix A. The model is comprised of seven dynamic states (x), three controlled inputs (u), and three measurable but uncontrolled inputs (w), which are noted in Fig. 1. The nonlinear model is expressed as

$$\dot{x} = f(x, u, w). \tag{1}$$

The first four states correspond to the absolute pressure in each of the four engine manifolds: intake (P_{im}), small-scroll exhaust (P_{ems}), large-scroll exhaust (P_{eml}), and post-turbine exhaust (P_{ex}). The fifth and sixth states are the burned gas fraction in the intake manifold (F_{im}) and small-scroll exhaust manifold (F_{ems}). These correspond to the proportion of combustion products present in each of the manifolds, which have a noticeable impact on combustion. The final state is the turbocharger shaft speed (N_{tc}).

The three controlled inputs (u) are the fuel quantity (u_f), EGR valve command (u_{egr}), and WG valve command (u_{wg}). The three measured but uncontrolled inputs (w) are the engine speed

(N_e), the ambient temperature (T_{amb}), and the ambient pressure (P_{amb}).

In production, the only measurable states are the intake mainfold pressure P_{im} and the turbocharger speed N_{tc}. Other outputs which may be measured are the intake manifold temperature T_{im} and the exhaust air-fuel equivalence ratio λ_{ex}. In development, additional instrumentation allows for consideration of the fault diagnosability under other sensor configurations.

2.3 Fault Model

The considered faults are leaks in each of the three main manifolds (IM, EMS, and EML). Manifold leaks can pose a serious problem for engine operation. Any leak will lead to decreased efficiency, and a large leak could result in a dramatic limitation of the maximum achievable acceleration. Further, exhaust manifold leaks, or intake manifold leaks when EGR is present, will lead to increased emissions and thus must be quickly detected under existing regulations [1].

Manifold leaks are modeled as a compressible flow through an orifice restriction as in [5]. Assuming that the manifold pressure is greater than the ambient pressure, the leak flow is given by

$$W_{leak} = \frac{P_m}{\sqrt{RT_m}} A \Psi \left(\frac{P_{amb}}{P_m} \right) \tag{2}$$

where

$$\Psi(\Pi) = \begin{cases} \sqrt{\frac{2\gamma}{\gamma-1}\left(\Pi^{\frac{2}{\gamma}} - \Pi^{\frac{\gamma+1}{\gamma}}\right)}, & \Pi \geq \left(\frac{2}{\gamma+1}\right)^{\frac{\gamma}{\gamma-1}} \\ \sqrt{\gamma\left(\frac{2}{\gamma+1}\right)^{\frac{\gamma+1}{\gamma-1}}}, & otherwise \end{cases} \tag{3}$$

where P_m, T_m are the manifold pressure and temperature respectively, P_{amb} is the ambient pressure, A is the leak area, R is the ideal gas constant, and γ is the ratio of the specific heats of the gas mixture, which, as in [7], is assumed constant and known. For simulated leaks, the area is assumed to be circular and is therefore described by its diameter.

Because the engine is turbocharged, manifold pressures can be assumed greater than ambient. This is observed in all of the operating points considered. It is thus a reasonable assumption that the leak flow is out of the manifold, and that a leak will reduce the manifold pressure, which, through the coupling present, will propagate to the rest of the model.

3 SYSTEMIC EFFECTS OF MANIFOLD LEAKS

In order to develop effective methods for isolating the considered types of leaks, it is important to first understand their effects on the system. As mentioned in Sec. 2.3, leaks produce a flow of material out of the manifold, which lowers that manifold's pressure. In a decoupled system, the source of the leak could be isolated by noting which manifold experienced a corresponding decrease in pressure compared to the model prediction. The engine air-path in the current work, however, exhibits significant coupling through the EGR path and the turbocharger. This section provides an investigation into the effects of this coupling on different manifold leaks. The investigation was carried out by simulating the considered model in the fault free case as well as with leaks of 2, 6, and 10 mm in each of the three manifolds. These simulations were performed for each of the 128 operating conditions shown in the speed-load map in Fig. 2. These points represent much of the breadth of engine operation, with the more frequently visited points being near the middle of the map. In addition, the analysis was repeated with the EGR valve mostly closed to decrease the impact of the state coupling that results from the EGR flow.

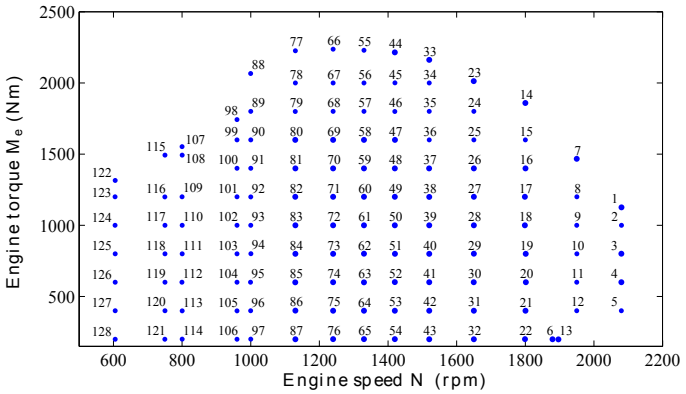

FIGURE 2. THE ENGINE SPEED AND TORQUE FOR THE OPERATING POINTS CONSIDERED.

The model used for fault detection/isolation is driven by the actual system inputs in an open-loop configuration. Thus, while the engine control system may change actuators to respond to a leak, the model will be driven by these new values which will in turn change the outputs of the model resulting in similar deviation as if no action were taken. Thus, the systemic effects of the leaks may be analyzed regardless of the control strategy used. Because of the different steady state points reached, it is possible that some variables in the closed loop system may exhibit different sensitivities to model error. Future work could address this extension.

3.1 Equilibria for Nominal EGR Values

From the model equations in Appendix A and [7], the coupling between model states as a result of internal feedback may be examined. A decrease in the intake manifold pressure results in increased flow through the EGR valve, less cylinder inflow, and accordingly less cylinder outflow. These changes in flow similarly decrease the pressure in the exhaust manifolds until a

new equilibrium is reached. A drop in exhaust manifold pressure, meanwhile, would accordingly decrease turbocharger shaft speed, which would decrease the pressure in the intake manifold. A leak in the small scroll exhaust manifold which feeds the EGR valve would also decrease intake manifold pressure via decreased EGR flow. Thus, regardless of the source of the leaks, the steady state effects on the system will be a decrease in each of the manifold pressures. This is verified in simulation of the model under different leak conditions at the operating points considered. Figures 3–5 show the deviation of the equlibiria as a result of the considered leaks projected into a few key planes. In Fig. 3, the value of $N_{tc,ss}$ as a function of $P_{im,ss}$ is seen to be a tight monotonic curve. This indicates that, in spite of other effects on the system, the equilibrium intake manifold pressure very nearly determines the equilibrium turbocharger speed, and vice versa. More extensive data from a similar engine exhibits a similar trend. While the trend does not hold across varying ambient conditions, a similar curve is observed at each simulated ambient condition. The curves in Figs. 4 and 5 are similar, but show significantly more spread depending on the operating point. Note that while there is some spread in the deviation of the equilibria depending on the leak type, the overall trend is very similar. By considering the outputs in Figs. 4 and 5, the spread in deviation based on leak-type is noticeable; however, in most cases, this is seen to be insufficient to differentiate between the leaks types.

An analysis was conducted to compare the average and maximum difference in the P_{im}, P_{ems}, P_{eml} and N_{tc} steady state values for leaks of the same size. This analysis was conducted across the 128 operating points for leaks of 2, 6, and 10 mm. Although exhaust pressures are not measurable in production, they provide insight into the system behavior which can be captured by other sensors. In the average case, none of these states show strong deviation (the greatest was 5.4%). The maximum deviations show that there exist conditions where, for large leaks, the effects of the leaks are as much as 16.2% different. Even then, the deviations are not much larger than the modeling errors observed in [7], where P_{im}, P_{ems}, P_{eml}, and N_{tc} average errors were 3.6%, 5.4%, 4.4%, and 4.2%, respectively (maximum errors were 14.3%, 16.5%, 28.8%, and 14.5%, respectively).

Given the similarity in the effects of the leaks when the sizes are known to be the same, it is be even more difficult to isolate the faults when the size of the leak is unknown, which is the case in actual operation. This is most easily explored using residuals based on an adaptive observer. As discussed in [5], adaptive observers are amenable to use for both detection and isolation of faults. The decrease in pressure as a result of a leak can be used to derive an adaptive state update law for a state observer:

$$\dot{\hat{x}} = f(\hat{x}, u, w, \hat{A}) \tag{4}$$

$$\dot{\hat{A}} = k_A(\hat{P}_{im} - \bar{P}_{im}) \tag{5}$$

$$\hat{P}_{im} = \hat{x}_1 \tag{6}$$

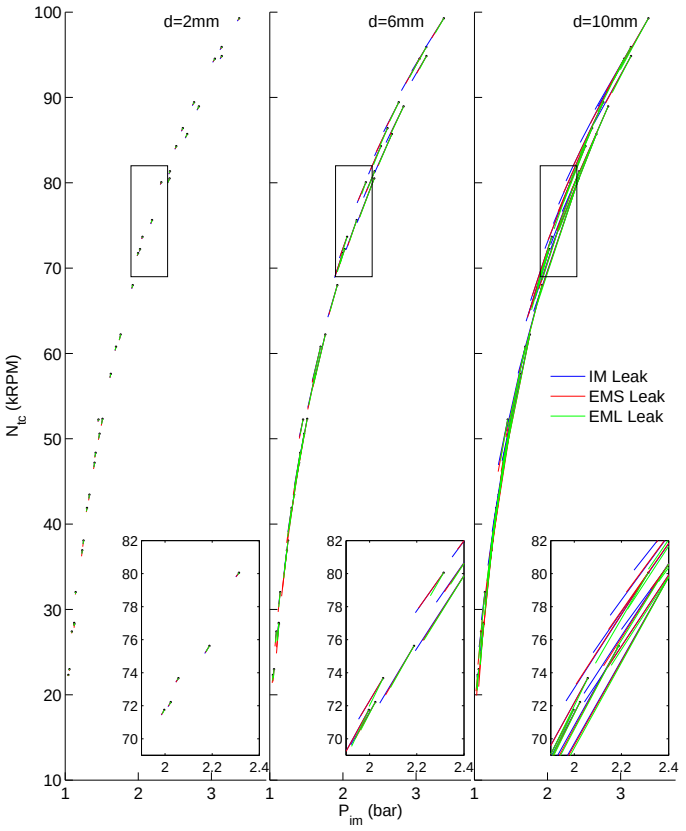

FIGURE 3. DEVIATION OF EQUILIBRIA WITH DIFFERENT LEAKS, PROJECTED ONTO THE $P_{IM} - N_{TC}$ PLANE. DOTS REPRESENT FAULT-FREE EQUILIBRIA, WHILE THE COLORED LINES EXTEND TO THE NEW EQUILIBIRUM VALUE.

where $\hat{A}$ is the estimated intake manifold leak area and k_A is the adaptive gain, which can be tuned for different operating conditions. This update is extended such that only non-negative values of $\hat{A}$ are allowed. This results in a vector of state estimates ($\hat{x}$), as well as other model outputs, given the estimated leak area.

By estimating a leak area which minimizes the error in intake manifold pressure ($\bar{P}_{im} - \hat{P}_{im}$), it is possible to estimate the intake manifold leak which is the most similar to the observed leak. The differences in the remaining states (P_{ems}, P_{eml}, and N_{tc}) will then give a measure of similarity for the two leaks. An analysis similar to the one for leaks of known size is presented in Tab. 1. As expected, the steady state errors have become even less pronounced. Even in the worst case, the only state that shows large disagreement is N_{tc}. The P_{ems} shows large descrepancies only for EMS leaks. However, for each of these, the errors are within the range of modeling errors seen in [7].

TABLE 1. DIFFERENCES BETWEEN THE MODEL WITH INTAKE LEAK ADAPTATION AND THE LISTED LEAK (ALL ENTRIES ARE PERCENT ERRORS). EACH COLUMN GIVES THE DIFFERENCE BETWEEN STEADY STATE FOR THE TWO LISTED LEAK TYPES FOR EACH CONSIDERED STATE.

State	IM2 mm	IM6 mm	IM10 mm	EMS2 mm	EMS6 mm	EMS10 mm	EML2 mm	EML6 mm	EML10 mm
Avg. ΔP_{im}	0.0000	0.0000	0.0000	0.0000	0.0000	0.0001	0.0000	0.0000	0.0001
Avg. ΔP_{ems}	0.0000	0.0000	0.0000	0.1962	1.6636	4.1482	0.0404	0.3437	0.8300
Avg. ΔP_{eml}	0.0000	0.0000	0.0000	0.0661	0.5727	1.4252	0.1562	1.3580	3.4188
Avg. ΔN_{tc}	0.0000	0.0000	0.0000	0.0623	0.6715	2.4882	0.0630	0.6329	2.1516
Max ΔP_{im}	0.0000	0.0002	0.0003	0.0001	0.0002	0.0010	0.0000	0.0004	0.0019
Max ΔP_{ems}	0.0000	0.0001	0.0003	0.3172	2.8342	7.7524	0.0862	0.7503	1.4980
Max ΔP_{eml}	0.0000	0.0001	0.0002	0.1263	1.0470	2.3853	0.3495	3.0435	6.5539
Max ΔN_{tc}	0.0000	0.0002	0.0005	0.3559	3.6958	12.5208	0.2353	2.3149	7.1761

3.2 Equilibria with Partially Closed EGR

Figure 6 demonstrates the degree of interconnectedness resulting from internal feedbacks such as EGR flow. These connections increase the difficulty in isolating faults. To reduce this effect, an analysis was performed with the EGR valve mostly closed. Even with a fully closed EGR valve, some leak flow will remain. Further, the considered model was only validated with operation in which the EGR valve was at least partially open. As a compromise between these considerations, the EGR valve was closed most of the way and it was investigated whether this had any improvement on the fault isolability.

The same analysis from the preceding section was conducted under this condition. Here the EGR valve was reduced to 5% open for each operating condition. Overall, it was found that in steady state this does not appreciably improve the isolability of these faults. The only conditions under which any appreciable improvement was seen were those with large leaks in the small scroll manifold. Using an adaptive observer which estimates the intake manifold leak area, the average error in the P_{ems} state was 4.1% for a 6 mm diameter leak and 9.4% for a 10 mm diameter leak, though even these values are close to the steady state modeling errors observed in [7] (5.4% average and 16.5% maximum error).

4 ANALYSIS

4.1 Residual-Based Isolation

Fault isolation is explored in the context of the adaptive observers mentioned previously. The states and outputs from such observers can be compared to measured values to form residuals for fault detection. In [5], such a residual is given by

$$r_{P,im} = \bar{P}_{im} - \hat{P}_{im}, \tag{7}$$

that is, a comparison of the measured intake manifold pressure (which was used for the adaptive feedback) to the estimate given from the adaptive observer. If the observer is capable of adapting the model such that the error in the pressure state is small, the residual based on this state will also be small. Since all leaks under the considered modes of operation reduce the manifold pressures, considering only residuals based on the pressure will not be able to differentiate between the leaks, because the residual will always be near zero. Whereas [5] considered only residuals based on the sensor used for feedback by the observer, this work considers residuals based on other states. For example, another residual can be constructed based on the turbocharger speed

$$r_{N,tc} = \bar{N}_{tc} - \hat{N}_{tc}. \tag{8}$$

Using residuals based on other model outputs, such as the turbocharger speed, allows for an improved fault isolation ability. Assuming stability of the observer, if the fault present is an intake manifold leak, the adaptation will result in a close estimate of the leak area and the model states and outputs will agree well with actual quantities. If a fault other than an intake manifold leak is present, the observer will estimate a leak area that minimizes the error in the intake manifold pressure. This will, in general, cause disagreement in the other states and outputs. From Tab. 1 and Fig. 4 and 5, it is seen that the P_{ems} and N_{tc} values show the greatest difference in effect, though these effects are still quite small compared to the observed modeling errors. Thus, while consulting a residual based on of a different state than the one used for feedback shows improved sensitivity to the difference between faults types, this improvement is still too small to be useful in the presence of typical model errors, such as those in [7].

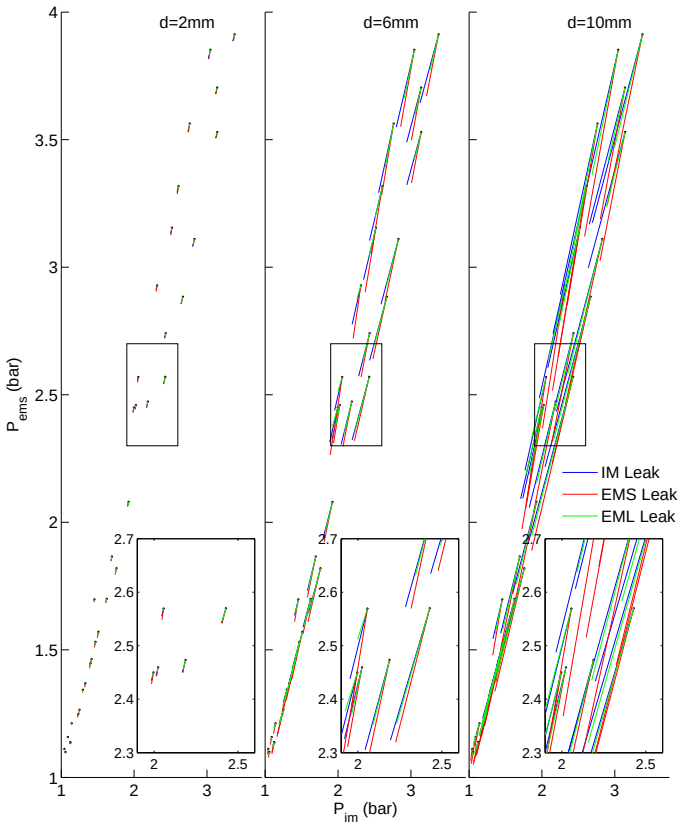

FIGURE 4. DEVIATION OF EQUILIBRIA WITH DIFFERENT LEAKS, PROJECTED ONTO THE $P_{IM} - P_{EMS}$ PLANE. DOTS REPRESENT FAULT-FREE EQUILIBRIA, WHILE THE COLORED LINES EXTEND TO THE NEW EQUILIBIRUM VALUE.

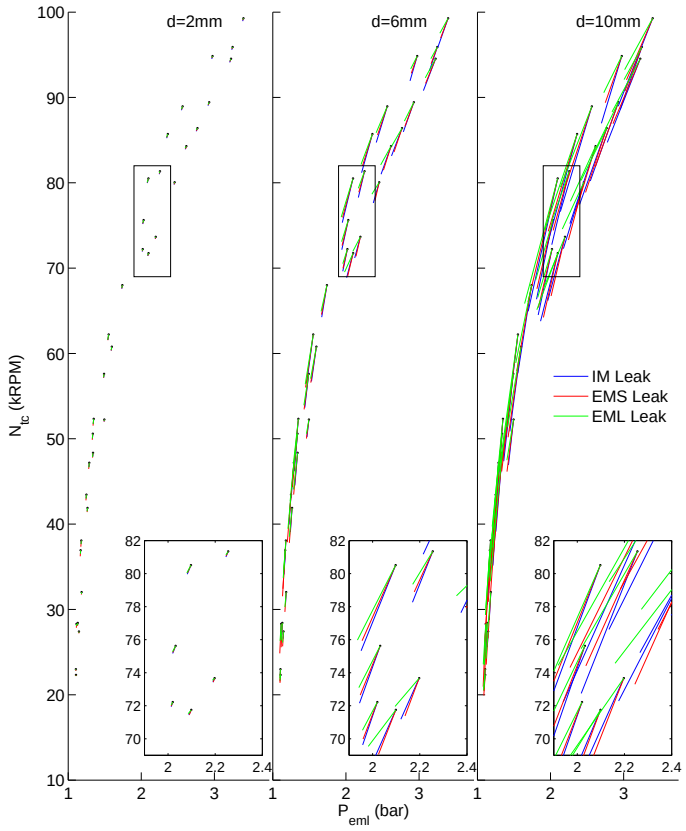

FIGURE 5. DEVIATION OF EQUILIBRIA WITH DIFFERENT LEAKS, PROJECTED ONTO THE $P_{EML} - N_{TC}$ PLANE. DOTS REPRESENT FAULT-FREE EQUILIBRIA, WHILE THE COLORED LINES EXTEND TO THE NEW EQUILIBIRUM VALUE.

4.2 Isolation Through Variance Monitoring

The preceding analysis indicates that, at steady state, it will not be possible to successfully isolate these types of leaks. As the engine operation changes, however, the variation of the signals contains information useful for successful isolation of the source of the leak. In particular, the adaptive observer system contains an estimate for an intake manifold leak area. Neglecting modeling error, if the leak in question is actually an intake manifold leak, the estimate for the leak area will approximate the actual leak area and will accordingly remain relatively constant throughout operation. If a leak is present in either exhaust manifold, the estimated intake leak area will still be selected to minimize the error in P_{im}. As the engine operation changes, this value is observed to change, since the modeled leak is not the leak actually present. Therefore a means by which these leaks may be successfully isolated is to consider the variation of the leak area estimate across the engine operation. Unfortunately, it may take a considerable amount of time to record enough data to be able to issue an isolation decision. This is because the operating condition will need to change enough to cause sufficient variation in the leak area estimate before an EM leak is differentiable from an IM leak. Nevertheless, the following analysis indicates that these types of leaks may be successfully isolated in some situations, which has not been shown in previous works.

In the following analyses, the time-response operation is not explicitly considered. While transient behavior may offer some additional insight into the type of fault present, fault detection systems often involve filtering of residuals to reduce the impact of noise, which also reduces the impact of the transient dynamics. Instead of considering the transient operation, this analysis instead investigates the steady state operation for each of the operating points considered. The means, standard deviations, and coefficients of variation are thus across these points, in steady state.

4.2.1 Effects of Model Errors

In this work, it is assumed that the faults which we attempt to isolate can be successfully detected. Previous works have demonstrated techniques for

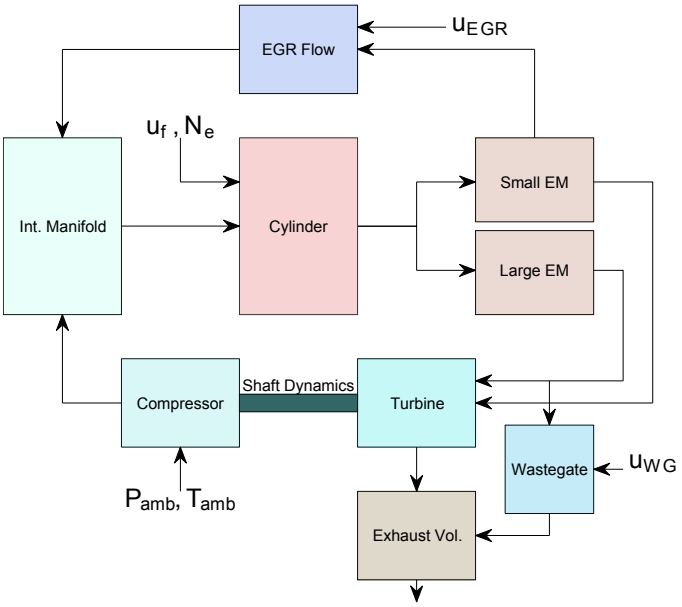

FIGURE 6. ENGINE MODEL BLOCK DIAGRAM DEMONSTRATING INTERCONNECTEDNESS. ARROWS DEMONSTRATE THE DIRECTION OF FLOWS AND THE EFFECTS OF INPUTS. DUE TO EFFECTS OF PRESSURES ON FLOWS AND OF FLOWS ON PRESSURE CHANGE, THE EFFECTS BETWEEN COMPONENTS ARE GENERALLY BIDIRECTIONAL.

successfully detecting IM leaks [5]. Since the effects of EM leaks are here shown to be very similar, it is concluded that the same techniques can detect this class of fault. Since the effects of the different leaks are seen to be quite similar at any given operating point, the proposed method for successful isolation is to consider the evolution of the estimated intake manifold leak area parameter as the engine operation changes. If the difference in variation of the area estimates for intake and exhaust manifold leaks is to be exploited, it must be analyzed in light of the variation in these estimates which is attributable to modeling error alone. To analyze this, the model with an adaptive observer which estimates an intake manifold leak is simulated using the actual measured value of the intake manifold pressure as the constant feedback signal.

Across the 128 operating points considered, the average leak area estimated due to the modeling error was approximately $6.29 \times 10^{-6}\,\mathrm{m}^2$ and the coefficient of variation (CoV) was approximately 1.8. This is a large degree of variation; however, it is mostly due to the small average leak area estimate. If a moderate sized leak is actually present, the effects of the modeling error on the variation across operating points will be much less. In particular, for a 10 mm leak in the EMS, the average leak area is $1.01 \times 10^{-4}\,\mathrm{m}^2$. Assuming that a similar amount of variation stems from the model error at this point, the CoV that is the result

TABLE 2. MEAN AND VARIATION FOR ESTIMATED LEAK AREAS ACROSS ENGINE OPERATING MAP.

	$\mu_A(\mathrm{mm}^2)$	$\sigma_A(\mathrm{mm}^2)$	CoV
Model Error	6.29	11.5	1.8
2 mm IM Leak	3.14	0.000224	7.14×10^{-5}
6 mm IM Leak	28.3	0.0012	4.11×10^{-5}
10 mm IM Leak	78.5	0.0024	3.05×10^{-5}
2 mm EMS Leak	3.78	1.529	.404
6 mm EMS Leak	34.9	14.5	.417
10 mm EMS Leak	101	44.52	.439
2 mm EML Leak	2.71	0.814	.301
6 mm EML Leak	25.1	7.40	.295
10 mm EML Leak	74.0	21.2	.286

TABLE 3. MEAN AND VARIATION FOR ESTIMATED LEAK AREAS ACROSS ENGINE OPERATING MAP, WITH REDUCED EGR VALVE POSITION.

	$\mu_A(\mathrm{mm}^2)$	$\sigma_A(\mathrm{mm}^2)$	CoV
2 mm IM Leak	3.14	0.00016	4.98×10^{-5}
6 mm IM Leak	28.3	0.00036	1.29×10^{-5}
10 mm IM Leak	78.5	0.0051	6.5×10^{-5}
2 mm EMS Leak	3.98	1.80	.451
6 mm EMS Leak	37.1	17.3	.467
10 mm EMS Leak	108	52.8	.491
2 mm EML Leak	2.33	0.644	.277
6 mm EML Leak	21.3	5.77	.271
10 mm EML Leak	60.9	15.8	.260

of the model error will only be around 0.15 while the CoV from the EMS leak is approximately 0.44 without model error. These results, as well as those in Sec. 4.2.2 are summarized in Tab. 2.

4.2.2 Passive diagnostics The isolation objective is to determine if the leak area estimate varies enough to be considered an exhaust leak. To assess this, the isolability was first explored, assuming no intervention is taken to ease the diagnosis. Examining the variation for the tests conducted, the CoV for the estimated leak area for intake manifold leaks was less than 10^{-4} while the CoV for small-scroll exhaust manifold leaks was around 0.4 and increased slightly with leak size. For large-scroll

manifold leaks, the CoV stayed roughly constant around 0.3. The trends in CoV indicate that larger EMS leaks show decreasing similarity to IM leaks, while larger EML leaks show increased similarity. Because it is not known how model error will behave in the presence of a leak, isolability is estimated by assuming that the variation based on model error is only present for IM leaks. This results in CoV's of 3.66, 0.406 and 0.146 for leaks of 2, 6, and 10 mm diameters, respectively. Since leaks smaller than 6 mm are seldom detectable, the CoV of 3.66 may be ignored since it corresponds to a leak that will not be detected. Based on Tab. 2, it appears that, in this scenario, EMS leaks of at least 6 mm could be isolated from IM leaks (since this is the smallest leak that resulted in a CoV greater than 0.406), while EML leaks do not show strong enough variation to be distinguished from IM leaks in the presence of modeling error (no leak size resulted in a CoV greater than 0.406).

4.2.3 Diagnosis with partially closed EGR

A similar analysis was conducted for the variation of the leak area estimates across leak areas with the EGR valve only 5% open. The CoV for IM leaks was similarly near 0, the CoV for EMS leaks increased slightly compared to the conditions for which the EGR valve was unmodified, and the CoV for EML leaks decreased slightly. These results are summarized in Tab. 3.

Thus there is some marginal improvement in isolability for EMS leaks if the EGR valve is partially closed, but it actually becomes more difficult to isolate the EML leaks under these conditions.

5 CONCLUSIONS

Fault isolation is an important aspect of fault diagnosis. It helps to decrease needed repair times and allows fault accommodation strategies specific to the particular type of fault to be employed. For these reasons, it is desirable to determine whether a leak has occurred on the exhaust or intake side of the engine. Building on the previous modeling work for the considered engine and making use of existing strategies and techniques in fault diagnosis, the feasibility of isolating these leak faults has been explored. In so doing, the interconnected nature of the engine air path was investigated. For passive diagnosis, the degree of similarity for the effects of the different leaks was too great for any steady state diagnostic strategy to successfully differentiate between the leaks. An approach that considers the operation of the engine across different conditions has been presented, which provides an improved means of successfully isolating intake and exhaust manifold leaks, by analyzing the variation of the estimated leak areas in an adaptive observer.

To attempt to reduce the interconnectedness and thereby ease the isolation problem, a similar analysis was carried out with the EGR valve mostly closed. This showed a marginal improvement for large leaks in the small scroll exhaust manifold, but not the large scroll exhaust manifold. In fact, closing the EGR valve makes the isolation of intake manifold leaks from large-scroll exhaust manifold leaks more difficult.

The effects of model errors on this approach are also explored. The proposed method shows promise for improved isolability, even in the presence of these errors and will be further validated in future work.

ACKNOWLEDGMENT

The authors would like to thank Justin Kollien, Jarrod Robertson, Jasman Malik, and Craig Savonen of Detroit Diesel Co. for their technical advice and assistance. Funding for this work was provided by Detroit Diesel Co.

REFERENCES

[1] Environmental Protection Agency. Control of Air Pollution From New Motor Vehicles and New Motor Vehicle Engines; Final Rule. *Federal Register*, 74(35):8321–8324,8332, 2009.

[2] N McDowell, G McCullough, X Wang, U Kruger, and G W Irwin. Fault Diagnostics for Internal Combustion Engines Current and Future Techniques. In *2007 SAE World Congress*, volume 2007, Detroit, MI, 2007. SAE.

[3] Carl Svärd, Mattias Nyberg, Erik Frisk, and Mattias Krysander. Automotive engine FDI by application of an automated model-based and data-driven design methodology. *Control Engineering Practice*, 21(4):455–472, April 2013.

[4] Ari Ingimundarson, Anna Stefanopoulou, and Denise McKay. Model-Based Detection of Hydrogen Leaks in a Fuel Cell Stack. *IEEE Transactions on Control Systems Technology*, 16(5):1004–1012, September 2008.

[5] Mattias Nyberg, Thomas Stutte, and Volker Wilhelmi. Model Based Diagnosis of the Air Path of an Automotive Diesel Engine. *Control Engineering Practice*, 12:513–525, 2004.

[6] Carl Svärd, Mattias Nyberg, Erik Frisk, and Mattias Krysander. Data-driven and adaptive statistical residual evaluation for fault detection with an automotive application. *Mechanical Systems and Signal Processing*, 45(1):170–192, March 2014.

[7] Mike J Hand III, Erik Hellstrom, Doohyun Kim, Anna Stefanopoulou, Justin Kollien, and Craig Savonen. Model and Calibration of a Diesel Engine Air Path with an Asymmetric Twin Scroll Turbine. In *Proceedings of the ASME 2013 Internal Combustion Engine Fall Technical Conference*, Dearborn, MI, USA, 2013. ASME.

APPENDIX A MODEL EQUATIONS

The model was developed previously in [7]. It consists of 7 dynamic states. For the 3 main pressure states the state equations are given by

$$\frac{dP_{im}}{dt} = \frac{R_a T_{im}}{V_{im}} \left(W_{egr} + W_c - W_{ei} - W_{im,leak}\right) \tag{9}$$

$$\frac{dP_{ems}}{dt} = \frac{R_{ex} T_{ems}}{V_{ems}} \left(\frac{1}{2} W_{eo} - W_{egr} - W_{ts} - W_{ems,leak}\right) \tag{10}$$

$$\frac{dP_{eml}}{dt} = \frac{R_{ex} T_{eml}}{V_{eml}} \left(\frac{1}{2} W_{eo} - W_{wg} - W_{tl} - W_{eml,leak}\right) \tag{11}$$

$$\tag{12}$$

where $W_{eo} = W_{ei} + W_f$. Much of the state coupling is the result of the internal feedback due to the turbocharger. The turbocharger speed state equation is given by

$$J_{tc} \frac{dN_{tc}}{dt} = M_t - M_c \tag{13}$$

where M is the power generated by the turbine or consumed by the compressor. The turbine and compressor powers, which determine the equilibrium turbocharger speed, satisfy the following relationships:

$$M_t \propto W_t / N_{tc} \tag{14}$$

$$M_c \propto W_c / N_{tc}. \tag{15}$$

In particular, an increase in turbine flow (W_t) increases the turbocharger speed, which increases the compressor flow. A decrease in turbine flow similarly decreases the compressor flow. This relationship results in much of the state coupling. The other main source of coupling is due to the EGR flow, which is described in [7], with the flow given by

$$W_{egr} = A(u_{egr}) \frac{P_{ems}}{\sqrt{R_{ex} T_{ems}}} \Psi \left(\frac{P_{im}}{P_{ems}}\right). \tag{16}$$

The flows exiting the EMS are the EGR flow and the small-scroll turbine flow. The flows exiting the EML are the large-scroll turbine flow and the WG flow. The corrected turbine flows satisfy the relationships

$$W_{tl,c} \propto (d_0 + d_1 r) \sqrt{1 - \left(\frac{P_{ex}}{P_{eml}}\right)^{d_2 + d_3 r}} \tag{17}$$

$$W_{ts,c} \propto r W_{tl,c} \tag{18}$$

$$r = f_r\left(N_{tc}, P_{ems}, P_{eml}, P_{ex}, T_{ems}, T_{eml}\right). \tag{19}$$

and the compressor flow satisfies

$$W_c \propto N_{tc}. \tag{20}$$

The turbine flows are corrected for operating conditions such that

$$W_{ts,c} = W_{ts} \frac{\sqrt{T_{ems}}}{P_{ems}} \quad W_{tl,c} = W_{tl} \frac{\sqrt{T_{eml}}}{P_{eml}} \tag{21}$$

and

$$W_t = W_{ts} + W_{tl}. \tag{22}$$